Infrared Physics & Technology 66 (2014) 1–5

Contents lists available at ScienceDirect

Infrared Physics & Technology

journal homepage: www.elsevier.com/locate/infrared

Stencil lithography of gold-black IR absorption coatings

Deep Panjwani [a], Mehmet Yesiltas [a], Simranjit Singh [a], Enrique Del Barco [a], R.E. Peale [a,*], Carol Hirschmugl [b], Julia Sedlemair [c]

[a] Department of Physics, University of Central Florida, Orlando, FL 32816, United States
[b] Department of Physics, University of Wisconsin-Milwaukee, Milwaukee, WI 53211, United States
[c] Synchrotron Radiation Center, University of Wisconsin-Madison, Stoughton, WI 53589, United States

HIGHLIGHTS

- We report infrared spectral microscopy of gold black patterns produced by stencil lithography.
- The spatial extent of strong IR absorption is somewhat smaller than the mask openings and visual appearance of the pattern.
- The edges of the patterns appear sharper at long-wave IR wavelengths than at shorter wavelengths.
- The patterned gold black is more conductive than for blanket depositions.

ARTICLE INFO

Article history:
Received 11 March 2014
Available online 14 May 2014

Keywords:
Gold black
Patterning
Shadow mask
Synchrotron radiation
Absorptance
IR detector

ABSTRACT

Gold black coatings are deposited through a stencil shadow mask to produce infrared-absorbing patterns with sub-mm lateral dimensions. Such dimensions match the characteristic pitch of Long Wave Infrared (LWIR) array bolometers. Infrared spectral imaging with sub-micron spatial resolution reveals the spatial distribution of absorption across the pattern.

1. Introduction

Gold black is a well-studied nano-structured metal film that shows strong broadband absorption throughout the visible to far-infrared range [1–5]. However, applications are limited due to mechanical fragility that makes patterning a challenge. The deposition process necessarily blankets large areas, so that it has usually been applied only to single element detectors [6]. Although sub-mm scale patterning by conventional metal lift-off using photoresist and solvents has been reported, no post patterning data regarding structure or absorption was given [7]. Our experience has been that the slightest contact with solvents collapses the film and destroys its intended properties [8]. Similarly, gold black cannot withstand heat treatment. Annealing at 150 °C for 1 h collapses the film. Aging even at room temperature coarsens the structure and affects absorption [9]. Despite these shortcomings, the low density (~0.02% of bulk) and correspondingly low heat capacity of gold black make it attractive for fast imaging-array applications [10], if patterning and stability limitations can be overcome.

We recently reported success of patterning *oxide over-coated* gold black through conventional lift-off in acetone solvent [11]. The oxide protected the gold black from complete collapse, and allowed patterning by lift-off. These patterns provided more than 90% absorptance in the 3–5 μm wavelength atmospheric window, but absorptance was reduced to ~70% in long-wave IR (LWIR), so there is reason to continue considering other methods. (Absorptance A is defined in terms of intensity according to $A + R + T = 1$, where R is reflectance and T is transmittance.)

Here we report patterning of gold black by stencil lithography. Typically in this method, patterns are transferred through shadow mask openings to the substrate or device in a single step, preferably in a non-contact mode. This attribute makes stencil lithography applicable for full wafer-scale fabrication [12] even on non-conventional substrates, such as freestanding bolometer membranes [13] and polymer surfaces [14]. Although stenciling has been widely popular for fabrication of milli- and micro-meter scale electronic circuits, recent advances have enabled patterning at

* Corresponding author. Tel.: +1 4072569884.
E-mail address: Robert.Peale@ucf.edu (R.E. Peale).

http://dx.doi.org/10.1016/j.infrared.2014.05.002
1350-4495/

nano scale with high-throughput and repeatability [15,16]. This method provides a low cost substitute for optical and electron-beam lithography, although blurriness around the edges (edge effect) is still a major shortcoming. The edge effect depends on source-mask distance, mask-substrate distance, and width of the mask openings [16].

In this work we prepared gold black patterns with sub-mm mask-substrate distances and found that stencil lithography preserves LWIR absorption. Differences in morphology are observed in comparison to blanket depositions. The patterns produced with stencil lithography are denser and more conductive than the blanket deposition. Absorption remains excellent out to at least 11 μm wavelength. Infrared imaging microscopy reveals a gradient of absorption near the pattern edges that is broader than would be inferred from the optical image. The infrared image showed sharper edges in the long-wave IR than in the mid-IR.

2. Experimental details

Our deposition system consists of a chamber that is evacuated by a diffusion pump. Once the pressure falls below 10^{-5} Torr, we back-fill the chamber with ultra-pure N_2 to a controlled pressure of ~300 m Torr. Parameters that affect film morphology include deposition rate, N_2 pressure, and mass of gold in the boat. A thermoelectric cooler (TEC) maintains the gold-coated substrate at −13 C. The cold side of the TEC, monitored with a thermocouple, is in direct contact with the substrate. The hot side of the TEC is attached to a water-cooled copper block using Apiezon N-type vacuum grease. Molybdenum evaporation boats with dimensions of 12 mm × 5 mm and 1 mm depth were filled with 400 mg of 99.9% gold. Substrate and Molybdenum boat are separated horizontally by 10 cm, and both face upward. The evaporation rate was similar for all depositions, averaging ~0.33 mg/s.

We use silicon substrates that have been coated by evaporation with an optically thick layer of gold on a 10 nm thick Cr sticking layer, so that absorptance may be determined from measurement of a simple reflectance spectrum ($T = 0$, $A = 1-R$). The stencil shadow mask was held at sub-millimeter distances from the substrate with layers of cellophane tape ("Scotch™") as spacers. Such tape has poor thermal conductivity, so that the mask is radiantly heated during the deposition while the substrate remains cold. This achieves preferential deposition on the substrate through the stencil windows. Nevertheless, gold black eventually accumulates on and clogs the mask apertures, so that cleaning in acetone after each use is required.

For conductivity measurements, coatings were deposited between two gold electrodes of 22.5 μm width and similar separation. A Ziess Ultra 55 scanning Electron Microscope (SEM) imaged cross sections to determine thickness, which was measured at the center of the pattern. Conductivity was obtained by dividing the slope of the I–V curve by this thickness. These were 2-point-probe measurements, so that contact resistance is present, though metal–metal contact resistance should be small.

Infrared reflection measurements were conducted using the Infrared Environmental Imaging (IRENI) mid-IR beam line at University of Wisconsin, Madison [17]. Synchrotron radiation provides much higher signal-to-noise ratio than can be obtained using usual globar IR sources. The end station of the IRENI beam line includes a Bruker Vertex 70 FTIR spectrometer connected to a Bruker Hyperion 3000 IR microscope, which is equipped with an FPA detector [18]. Each image spans the field of view with 96 × 96 pixels, each of which is 0.54 μm × 0.54 μm in area, giving diffraction-limited spatial resolution over the full mid-infrared spectral range of 900–3700 cm^{-1}. Reflectance spectra were collected with a 20×, 0.65 numerical aperture (NA) Schwarzschild objective attached to the microscope, and with 4 cm^{-1} spectral resolution. Finally, the IRidys (Infrared Imaging & Data Analysis) program, which operates within the commercial IGOR Pro software package, was used to extract spectral information from different pixels [19].

3. Results & discussion

When the height of the shadow mask is optimum, well-defined and reproducible patterns are obtained. Fig. 1 presents optical microscope images of two different patterns fabricated using circular and square shadow masks, respectively, at sub-mm mask heights above the substrate surface. All deposition parameters were similar for both patterns, except that the pattern in Fig. 1b is produced with nearly twice the mask-substrate separation as that in Fig. 1a. Significant differences appear in thickness, morphology, and edge definition. The Fig. 1b coating appears thinner and its edges are fuzzier. In other words, the closer the shadow mask is to the substrate, the sharper are the edges and the thicker is the resulting pattern. The thickness of the pattern in Fig. 1(a) exceeds ~10 μm, which gives high far-IR absorption. However, such thick coatings are more prone to mechanical damage. The upper structure of the thick coating is blown off immediately when exposed to a stream of nitrogen gas coming out of a 4-mm internal-diameter

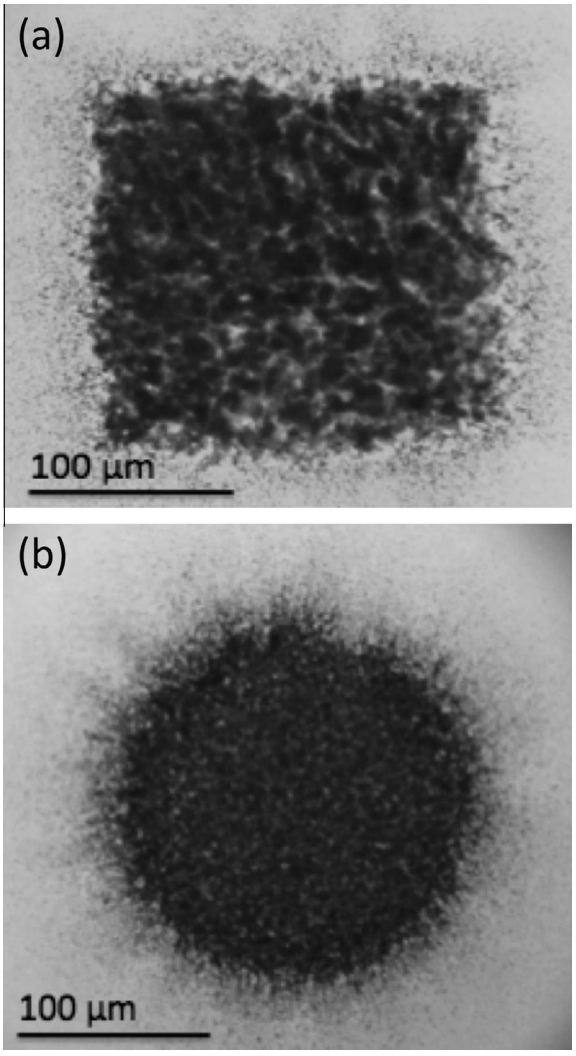

Fig. 1. Optical microscope images of gold black patterns produced with shadow mask. The mask-substrate separation was twice larger for the circular pattern.

nozzle at 70 liters/min flow rate from a distance of approximately 1 cm. The sub-structure of the coating adheres well to the Si substrate. Patterns of ~5 μm thickness, such as shown in Fig. 1(b), survived the nitrogen-jet test.

Fig. 2a presents SEM images of coatings made by blanket deposition without a mask. The average feature size exceeds that produced when a shadow mask is used (Fig. 2b), and these blanket depositions appear less dense. In each case, the substrate was cooled to −13 °C. However, the mask shades the substrate from radiant heating, which allows the substrate to be colder than without the mask, so that cryo-pumping enhances the accumulation. Moreover, the relative warmth of the mask aperture may focus and enhance the gold-black flux through the apertures. That the patterned films are thinner but denser we attribute to the exclusion by the mask of long chains of gold black particles that link together before reaching the mask. The smaller chains that make it through the aperture are able to pack more closely together. When thermally conducting spacers are used, the temperature differential between mask and substrate decreases, and the patterns produced are sparse and discontinuous, while deposits on the mask itself are heavy. Similarly, we expect from these experiments that the thermal conductivity and infrared absorptivity of the mask material will affect coating morphology. Additionally, we note that smaller mask openings produce pattern edges that are not as abrupt.

The *I–V* curves for both blanket depositions and patterns were linear, which shows that their behavior is ohmic. The patterned gold black showed twice the conductivity of the blanket deposition, in agreement with the tighter packing observed in Fig. 2b. Larger mask-substrate separations give lower conductivity due to reduced gold-black flux through the mask aperture. Coatings with higher conductivity are expected to have higher absorption coefficient [20]. Therefore, the higher conductivity of the patterned coatings allows them to be thinner, and hence more robust. However, if the density becomes too high, the film may begin to look like a bulk metal, for which reflection increases with conductivity. Mask height can be optimized to achieve morphology with desired density and conductivity characteristics.

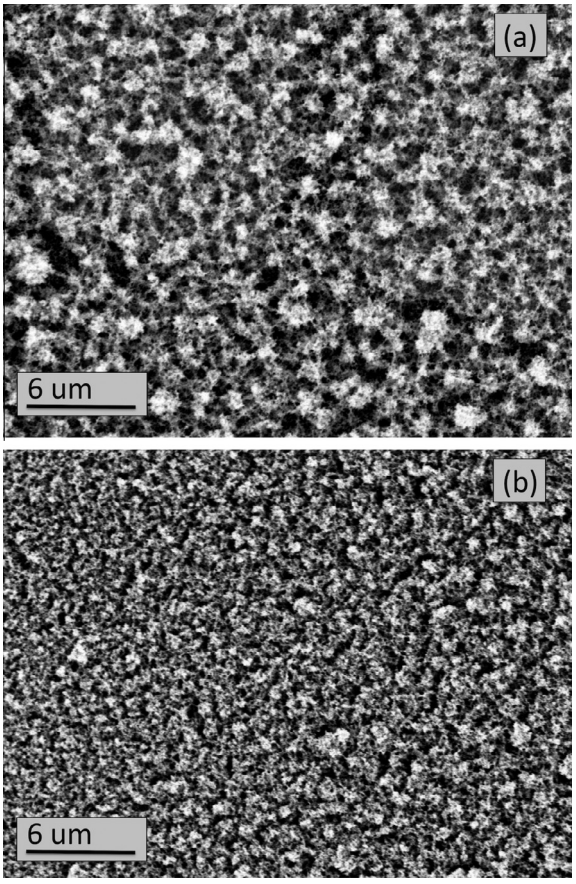

Fig. 2. SEM image of gold black produced (a) without and (b) with shadow mask at height of 0.3 mm.

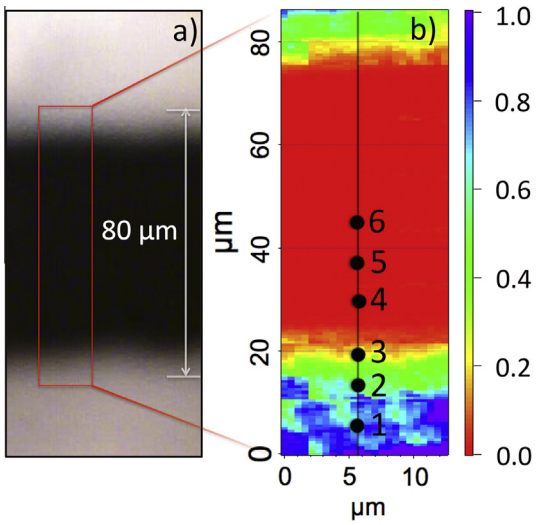

Fig. 3. (a) Optical microscope image of gold black pattern. (b) Spectrally-integrated IR reflectance microscope image of the same sample. Numbered dots indicate where spectra are sampled. The color scale indicates reflectance, which is integrated over the range 970–3700 cm^{-1}. (For interpretation of the references to color in this figure legend, the reader is referred to the web version of this article.)

The spatial distribution of reflectance near the edge of a stripe pattern (Fig. 3a) is presented in Fig. 3b. The coating thickness is comparable to that in Fig. 1b. The dimensions of the gold black pattern are 85 μm × 13 μm, as determined from the optical microscope image Fig 3a. The color scale (online) gives the[1] spectrally integrated reflectance over the wavenumber range 900–3700 cm^{-1} (11.1–2.7 μm wavelength). The optical image shows blurred edges, which are transition regions of intermediate reflectance that are colored green in the IR image. Strongly absorbing regions of less than 5% reflectance are red, while the ~90% reflecting gold substrate surface is blue. The width of the mask aperture is 80 μm, but the region of maximum absorption extends over a width of only 52 μm. In other words, the transition region on each side is 14 μm wide, which is not apparent in the visible-band optical image.

Fig. 4 presents reflectance spectra extracted from the six different pixels labeled in Fig. 3. Pixel 1 is located on the bare gold substrate and shows the expected high reflectance from the gold surface. The decrease toward higher wavenumbers can be attributed to scattering by sparse gold black strands at the very edges of the deposition. Pixel 2 and 3 are from the transition zone of intermediate reflectance and show increasing absorption. Artifacts due to atmospheric water vapor and carbon dioxide are evident in spectra from pixel 1 and 2. Spectra from pixels 4 to 6 are well within the main deposition and show strong absorptance across the spectrum. Reflectance at pixel 5 is less than 1%. At pixel 6, signal is null, resulting in flat reflectance coincident with the horizontal axis. Although such thin coatings may lack high absorptance in the far-IR [20], they do retain high absorptance out to at least

[1] For interpretation of color in Fig. 3, the reader is referred to the web version of this article.

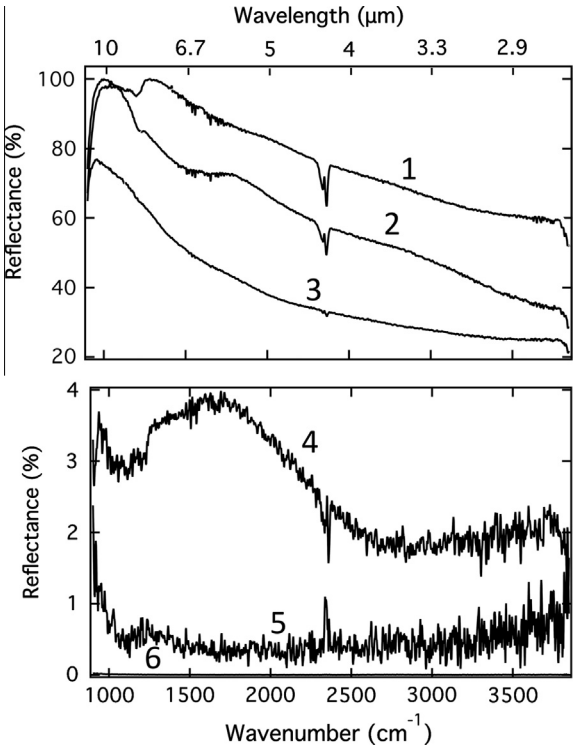

Fig. 4. Reflectance spectra extracted from six different pixels numbered as in the infrared image Fig. 3.

11 μm wavelength, while they are more robust than thicker coatings.

Fig. 5 presents the infrared image at two different wavelengths for the same pattern as in Fig. 3a. At 2.7 μm the edges appear fuzzy with a broad transition region (yellow–green). The edges are sharper at 11.1 μm, with transition regions only ~4 μm wide. This is because at longer wavelengths there is less absorption and/or scattering by the sparse particle distributions at the edges of the pattern. The mask distance from the device can be optimized to attain effective absorbing area (red), similar to that of pixel size. Any lateral spreading between the pixels should cause less thermal crosstalk between pixels at long-wave-IR than at mid-IR wavelengths.

Fig. 6 compares reflectance line profile scanned horizontally at the centers of each image in Fig. 5. The width of the low-reflectance region (red) at 2.7 μm and 11.1 μm is 52 μm and 48 μm, respectively. This indicates that although the pattern edges appear indistinct at short wavelengths, they are sharp in LWIR. On the other hand, the corners of square patterns were less distinct in the LWIR,

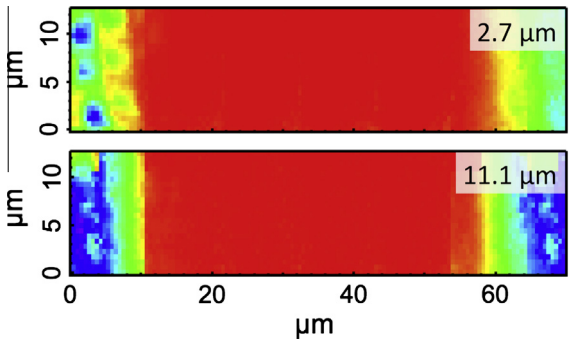

Fig. 5. Infrared image of gold-black pattern at indicated wavelengths.

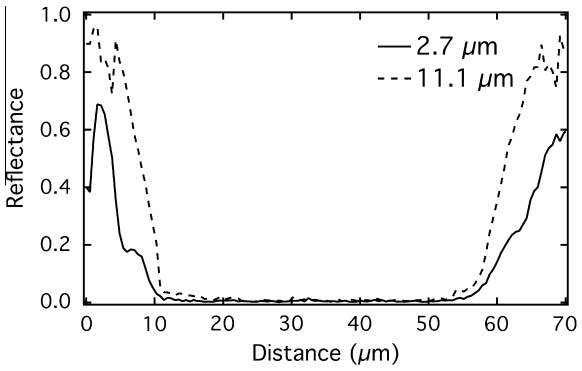

Fig. 6. The reflectance profile scanned horizontally across the centers of the IR images in Fig. 5.

so that the patterns appeared more circular. The 5 μm thickness appears adequate to achieve high absorptance in the long-wave IR.

4. Conclusion

Scanning Electron Microscopy revealed that the morphology of a gold-black pattern produced with a shadow mask is more closely packed than for blanket depositions. *I–V* measurements showed higher conductivity for those mask-defined patterns. The substrate-mask separation can be optimized to attain desired density and conductivity. Results presented here suggest the possibility of preparing gold black patterns with lower thickness than for blanket depositions with similarly high absorptance in the LWIR. This may be advantageous since thinner depositions are more robust mechanically. Synchrotron-based IR spectral imaging with submicron spatial resolution revealed absorbing areas significantly smaller than indicated by the mask openings and apparent optical dimensions of the patterns. The edges of the patterns are sharper at LWIR than at shorter wavelengths.

Conflicts of interest

The authors declare that there are no conflicts of interest.

Acknowledgments

UCF authors were supported in part by a grant from the Florida High Technology Corridor Program (I-4). This work is based in part upon research conducted at the Synchrotron Radiation Center, which is primarily funded by the University of Wisconsin-Madison with supplemental support from facility Users and the University of Wisconsin-Milwaukee. This work is based on research conducted at the IRENI beam line, whose construction and development were supported by NSF award #0619759 and NSF CHE-1114233. S.S. and E.d.B. acknowledge support from the NSF-ENG Collaborative Research grant ECCS-1001755.

References

[1] L. Harris, R.T. McGinnies, B.M. Siegel, The preparation and optical properties of gold blacks, J. Opt. Soc. Am. 38 (1948) 582–589.
[2] L. Harris, A.L. Loeb, Conductance and relaxation time of electrons in gold blacks from transmission and reflection measurements in the far infrared, J. Opt. Soc. Am. 43 (1953) 1114–1118.
[3] L. Harris, The transmittance and reflectance of gold black deposits in the 15- to 100- micron region, J. Opt. Soc. Am. 51 (1961) 80–82.
[4] L. Harris, P. Fowler, Absorptance of gold in the far infrared, J. Opt. Soc. Am. 51 (1961) 164–167.
[5] W. Becker, R. Fettig, A. Gaymann, W. Ruppel, Black gold deposits as absorbers for far infrared radiation, Phys. stat. sol. (b) 194 (1996) 241–255.

[6] J. Lehman, E. Theocharous, G. Eppeldauer, C. Pannell, Gold-black coatings for freestanding pyroelectric detectors, Measur. Sci. Technol. 14 (2003) 916–922.
[7] M. Hirota, Y. Nakajima, M. Saito, M. Uchiyama, 120 × 90 element thermoelectric infrared focal plane array with precisely patterned Au-black absorber, Sens. Actuator, A 135 (2007) 146–151.
[8] L. Harris, J.K. Beasley, The infrared properties of gold smoke deposits, J. Opt. Soc. Am. 42 (1952) 134–140.
[9] Donna J. Advena, Vincent T. Bly, J. Thomas, Cox, deposition and characterization of far-infrared absorbing gold black films, Appl. Opt. 32 (1993) 1136–1144.
[10] Biao Li, Design and simulation of an uncooled double-cantilever microbolometer with the potential for ~mK NETD, Sens. Actuators A 112 (2004) 351–359.
[11] Deep Panjwani, Mehmet Yesiltas, Janardan Nath, D.E. Maukonen, Imen Rezadad, Evan M. Smith, R.E. Peale, Carol Hirschmugl, Julia Sedlmair, Ralf Wehlitz, Miriam Unger, Glenn Boreman, Patterning of oxide-hardened gold black by photolithography and metal lift-off, Infra. Phys. Technol. 62 (2014) 94–99.
[12] Veronica Savu, Marc A.F. van den Boogaart, Juergen Brugger, Julien Arcamone, Marc Sansa, Francesc Perez-Murano, Dynamic stencil lithography on full wafer scale, J. Vac. Sci. Technol. B 26 (2008) 2054–2058.
[13] N. Nelms, G. Butcher, O. Blake, R. Cole, C. Whitford, A. Holland, Focal plane array for the GERB instrument, Proc. SPIE 5251 (2004) 136–141.
[14] Nao Takano, Lianne M. Doeswijk, Marc A.F. van den Boogaart, Janko Auerswald, Helmut F. Knapp, Olivier Dubochet, Thomas Hessler, Jurgen Brugger, Fabrication of metallic patterns by microstencil lithography on polymer surfaces suitable as microelectrodes in integrated microfluidic systems, J. Micromech. Microeng. 16 (2006) 1606–1613.
[15] O. Vazquez-Mena, G. Villanueva, V. Savu, K. Sidler, M.A.F. van den Boogaart, J. Brugger, Metallic nanowires by full wafer stencil lithography, Nano Lett. 8 (2011) 3675–3682.
[16] Serap Aksu, Ahmet A. Yanik, Ronen Adato, Alp Artar, Min Huang, Hatice Altug, High-throughput nanofabrication of infrared plasmonic nanoantenna arrays for vibrational nanospectroscopy, Nano Lett. 10 (2010) 2511–2518.
[17] C.J. Hirschmugl, K.M. Gough, Fourier transform infrared spectrochemical imaging: review of design and applications with a focal plane array and multiple beam synchrotron radiation source, Appl. Spectrosc. 66 (2012) 475–491.
[18] M.J. Nasse, M.J. Walsh, E.C. Mattson, R. Reininger, A. Kajdacsy-Balla, V. Macias, R. Bhargava, C.J. Hirschmugl, High resolution Fourier-transform infrared chemical imaging with multiple synchrotron beams, Nat. Meth. 8 (2011) 413–416.
[19] M.J. Nasse, B. Bellehumuer, S. Ratti, C. Olivieri, D. Buschke, Jayne Squirrell, Kevin Eliceiri, B. Ogle, C. Schmidt Patterson, M. Giordano, C.J. Hirsch, Opportunities for multiple-beam synchrotron-based mid-infrared imaging at IRENI, Vib. Spectrosc. 60 (2012) 10–15.
[20] W. Becker, R. Fettig, W. Ruppel, Optical and electrical properties of black gold layers in the far infrared, Infra. Phys. Technol. 40 (1999) 431–445.